ARTICLES

Vibrational and Rotational Distributions of the CH($A^2\Delta$) Product of the $C_2H + O(^3P)$ Reaction Studied by Fourier Transform Visible (FTVIS) Emission Spectroscopy

Viktor Chikan and Stephen. R. Leone*

Departments of Chemistry and Physics, and Lawrence Berkeley National Laboratory, University of California, Berkeley, California 94720-1460

Received: June 24, 2005; In Final Form: October 2, 2005

The $C_2H + O(^3P) \rightarrow CH(A) + CO$ reaction is investigated using Fourier transform visible emission spectroscopy. The $O(^3P)$ and C_2H radicals are produced by simultaneous 193 nm photolysis of SO_2 and C_2H_2 precursors, respectively. The nascent vibrational and rotational distributions of the CH(A) product are obtained under time-resolved, but quasi-steady-state, conditions facilitated by the short lifetime of the CH(A) emission. The vibrational temperature of the CH(A) product is found to be appreciably hotter (2800 ± 100 K) than the rotational distributions in the $v' = 0$ (1400 ± 100 K) and $v' = 1$ (1250 ± 250 K) levels. The results suggest that the reaction may proceed through an electronically excited $HCCO^{\ddagger}$ intermediate; moreover, the vibrational excitation compared to rotational excitation is higher than expected based on a statistical distribution of energy and may be the result of geometrical changes in the transition state. The CH(A) emission is also observed in a C_2H_2/O/H reaction mixture using a microwave discharge apparatus to form O atoms, with subsequent H atom production. The nascent rotational and vibrational distributions of the CH(A) determined by the microwave discharge apparatus are very similar to the CH(A) distributions obtained in the photodissociation experiment. The results support the idea that the $C_2H + O(^3P)$ reaction may play a role in low-pressure C_2H_2/O/H flames, as previously concluded.

Introduction

The $CH(A^2\Delta) \rightarrow CH(X^2\Pi)$ transition at 430 nm has been long identified as a major source of blue emission in hydrocarbon rich flames and in C_2H_2/O/H atomic flames.[1] The first proposed mechanism came from Gaydon,[2,3] who suggested that the CH(A) emission is due to the $C_2 + OH \rightarrow CH + CO$ reaction. This proposed mechanism was supported by the observation that the [CH(A)]/[C_2][OH] ratio in hydrocarbon flames was independent of several flame parameters. Brenig et al.[4] rejected the above mechanism by showing that no CH(A) production can be observed in systems containing C_2 and OH in the absence of O atoms. Several groups[5−7] suggested that the O atoms play an essential role in the CH(A) production, which could be explained by the following reaction

R1

$$C_2H + O(^3P) \rightarrow CH(A) + CO \quad (-11 \text{ kcal/mol}, -46 \text{ kJ/mol})$$
$$\rightarrow \text{other channels}$$

Similar to the above reaction, the ethynyl radical can also react with molecular oxygen resulting in CH(A) as first suggested by Renlund et al.[8,9]

R2

$$C_2H + O_2 \rightarrow CH(A) + CO_2 \quad (-19 \text{ kcal/mol}, -80 \text{ kJ/mol})$$
$$\rightarrow \text{other channels}$$

Both of these reactions are important in hot hydrocarbon flames; however, Devriendt and Peeters[6] showed by direct comparison that the room-temperature rate constant of R1 (1.8×10^{-11} cm^3 molecule^{-1} s^{-1}) is about 500 times greater than the rate constant of R2 (3.6×10^{-14} cm^3 molecule^{-1} s^{-1}). They concluded that R1 is the major, if not dominant, source of CH* production in hydrocarbon-rich flames.[6]

Previously,[10] we investigated the CO product of the $C_2H + O(^3P)$ reaction by time-resolved FTIR spectroscopy. The branching ratio of the CH(A)/CH(X) channels was inferred to be relatively large (60%) compared to estimates from previous kinetic measurements (8%).[6,11] In addition, the vibrational distribution of the CO product shows a slight inverted behavior, suggesting preferential disposal of energy into the vibrational degrees of freedom for both the CH(X) and CH(A) channels. This paper investigates the dynamics of the R1 reaction via the CH(A) product by FTVIS emission spectroscopy. The C_2H and $O(^3P)$ radicals are generated by photodissociation of C_2H_2 and SO_2 precursors, respectively. At low pressures, fitting the CH(A) product spectra allows the extraction of nascent vibrational and rotational populations of the CH(A) product. From the relatively high vibrational excitation of the CH(A), the results suggest that the transition state geometry may play an important role in determining the final product state distribution. In addition, the conditions present in low-pressure C_2H_2/O/H flames are simulated using a microwave discharge apparatus. Under similar conditions to the photodissociation experiment, the nascent CH(A) rotational and vibrational distributions from the microwave discharge experiment are obtained. The CH(A) distributions from the microwave discharge experiment are very similar to the CH(A) distributions from the photodissociation experiment, in agreement with a previously

* To whom correspondence should be addressed. E-mail: srl@berkeley.edu.

10.1021/jp053444w CCC: $30.25
Published on Web 11/08/2005

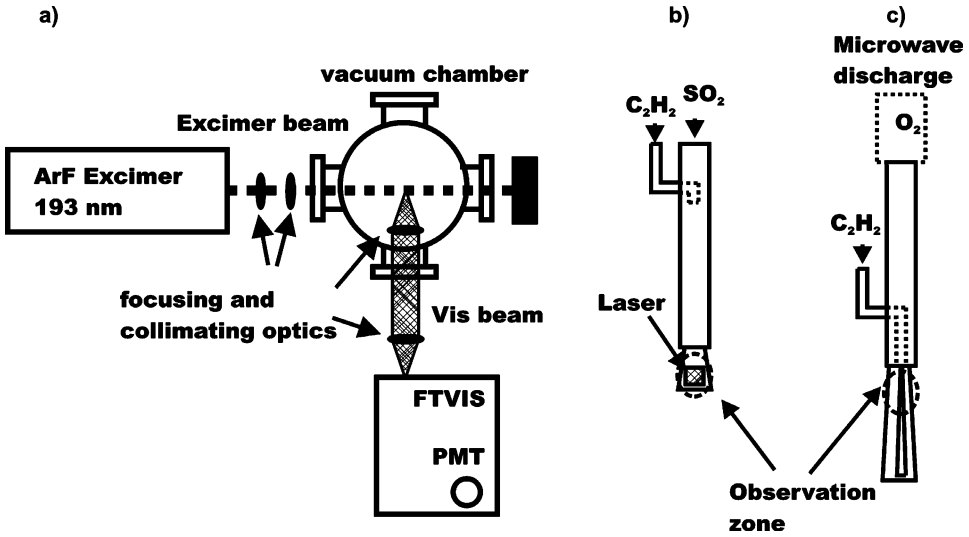

Figure 1. (a) Simplified schematic of the time-resolved FTVIS apparatus used in this study. The gas is introduced through an effusive source (b) perpendicular to the plane of the schematic at the middle of the vacuum chamber. The excimer laser beam path is indicated by a dashed line. (c) Microwave discharge reactor: the $O(^3P)$ atoms are generated in a microwave discharge from a flow of O_2 and combined with the C_2H_2 flow in the observation zone of the FTVIS.

proposed mechanism[6,7] for the CH(A) formation in C_2H_2/O/H flames. We propose that the obtained nascent distribution of CH(A) may be used to follow the formation of C_2H radicals in low-pressure flames.

Experimental Section

The experimental apparatus is described in detail elsewhere,[10,12] and only a brief description is given here. The experimental setup (Figure 1a) consists of a vacuum chamber, FTVIS spectrometer, and a 193 nm ArF excimer laser. The vacuum chamber contains the fast flow reactor (Figure 1b) made of a stainless steel tube about 1 cm in diameter, where the precursor molecules (SO_2 and acetylene) are introduced into the chamber. The flow of SO_2 and acetylene mixture is intersected with the excimer laser beam focused to a 1 cm^2 spot. The SO_2 and C_2H_2 flows are 120 and 180 sccm, respectively. An Ar flow, which is introduced at the windows, is helpful to keep the windows clean and to confine the reagent flows in the observation region, increasing the collisions between C_2H and O radicals. The energy of the laser beam is kept below 60 mJ/pulse/cm^2 to lower the probability of multiphoton processes.[13] The visible emission of the reaction is collimated and focused on the FTVIS spectrometer. The interferometric detection requires limiting the field of view[14] to enhance the spectral resolution of the FTVIS. This is achieved by placing an iris in front of the FTVIS, which also helps reduce the stray light. The FTVIS detection uses a blue-sensitive photomultiplier tube. Interference filters (e.g., 430 nm) are used to enhance the sensitivity of the FTVIS apparatus and to speed up the data collection time by reducing the number of points in the interferograms.[14] The spectra are normalized by the instrument response function determined from the emission of a known calibration lamp.

The microwave discharge apparatus is identical to the apparatus described previously,[12] and it is very similar to the photodissociation apparatus above, with the exception of using a microwave discharge reactor to generate O atoms from O_2 molecules. Figure 1c shows the reactor used in the microwave discharge experiments. The microwave discharge of oxygen molecules takes place in a quartz tube, efficiently producing $O(^3P)$ atoms. The $O(^3P)$ atoms are mixed downstream with the flow of C_2H_2. The acetylene flow is kept relatively low compared to the O_2 flow so the flow does not become divergent.

For the photodissociation experiment, the C_2H radicals are generated by 193 nm photolysis of acetylene (99.6%), which is purified by an activated carbon trap in order to remove the residual acetone stabilizer from the C_2H_2 reagent flow. The trap is evacuated overnight before each experiment to ensure efficient removal of the acetone. 193 nm photolysis of the residual acetone would produce vibrationally excited CO (98% yield of total CO).[15] For these experiments, operating the instrument in FTIR mode, no CO(v) signal is observed from the photolysis of residual acetone during the experiments. The $O(^3P)$ is produced by photolysis of SO_2 (anhydrous, 99.98%) or microwave discharge of O_2 (99.998%). Pressure is measured using capacitance manometers. The gas flows are regulated by needle valves and measured by standard mass flow meters.

Results and Discussion

Photodissociation Experiment. In this study, the CH(A) product of the $C_2H + O(^3P)$ reaction is studied. The radicals are generated by 193 nm photodissociation of SO_2 and C_2H_2 molecules. Figure 2 shows the laser power dependence of the CH(A) fluorescence and a SO_2 fluorescence signal[16] taken separately in the absence of C_2H_2, both acquired through a 430 nm interference filter. The CH(A) signal is quadratic (Figure 2a), as expected from the $C_2H + O(^3P)$ reaction. As a reference, the laser power dependence of the SO_2 fluorescence during the SO_2 predissociation at 193 nm is shown in Figure 2b, which indicates a linear dependence. The SO_2 is strongly dissociated with 193 nm excitation, however, a small portion of the electronically excited SO_2 may emit back to the ground state by fluorescence. It is also possible that the recombination of the SO with O can produce electronically excited SO_2, which would also relax through fluorescence, but the power dependence of that process is expected to be quadratic. The SO_2 fluorescence is much weaker at 430 nm, because the SO_2 is strongly predissociating at excitation wavelengths shorter than 210 nm to produce $O(^3P)$ and SO. In addition, the SO_2

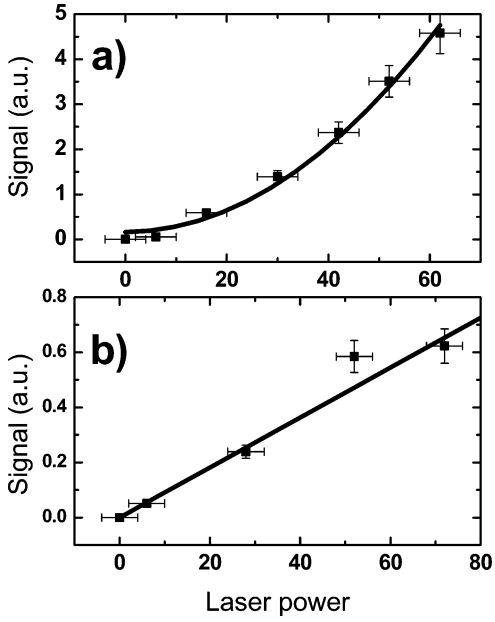

Figure 2. (a) Power dependence of the CH(A) signal taken with an interference filter. The data are fitted with a simple quadratic function indicated by the solid line. (b) Power dependence of the SO_2* fluorescence taken with the same interference filter without C_2H_2 introduced. The data are fitted with a simple linear function indicated by the solid line.

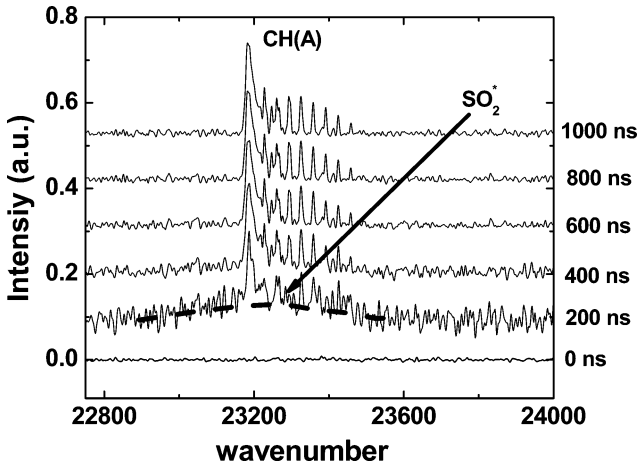

Figure 3. Time-resolved visible emission spectra of the CH(A) from the $C_2H + O(^3P)$ reaction process. The total pressure is 100 mTorr (13 Pa) with the balance due to Ar in the detection volume of the instrument. The laser fluence is 60 mJ cm^{-2} $pulse^{-1}$. The data are taken at 4 cm^{-1} spectral and 250 ns temporal resolution. For better comparison, the data from 250−1000 ns are normalized to the area in the spectrum. The dashed line indicates the initial appearance of the SO_2 fluorescence. Both spectral features are convolved with the transmission curve of a 430 nm interference filter.

fluorescence is detected at the red edge of the SO_2 emission band.

The time evolution of a low-resolution (4 cm^{-1}) visible spectrum of the CH(A) species from the $C_2H + O(^3P)$ reaction is presented in Figure 3. The spectra are taken every 200 ns and normalized to the area to allow a comparison of the spectra taken at different times. A broad, unresolvable spectral feature appears during the first 200 ns, which is due to the SO_2 fluorescence from the excitation of SO_2. The spectral feature disappears within 200 ns, which agrees very well with the instrument-response-limited emission lifetime of SO_2*. In addition, this spectral feature is present without the addition of the C_2H precursor (C_2H_2) to the photolysis mixture. The CH(A) emission at early times and later times is identical, suggesting a quasi-steady-state equilibrium between the production of CH(A) and the removal of CH(A), whereby the state distribution is unchanging due to the short radiative lifetime.

To extract populations from the spectral data, two main conditions are sought. First, the spectrum observed from a photodissociation process, or from a reaction such as the $C_2H + O(^3P)$ reaction, has to be nascent. Second, the populations of a particular transition in the product should not be influenced by intramolecular processes such as predissociation. Under the experimental circumstances, both of these conditions are valid for reasons described below.

The time-resolved signal in Figure 3 shows no indication of rotational relaxation. While this result is not definite proof for the absence of rotational relaxation, since the observed CH(A) is a result of quasi-steady-state conditions between collisions that produce the reaction and the collisions leading to relaxation, estimates suggest that the product state results are not relaxed. Previous studies[17,18] show that after photolysis the initial amount of $C_2H(A)$ and the vibrationally hot C_2H is less than 50%. The actual observed fraction of CH(A) from $C_2H(A) + O(^3P)$ may be much lower for several reasons. The exothermicity of the reaction ($C_2H(A) + O(^3P)$) would be about 4000 cm^{-1} higher, which is enough to access other vibrational states, such as CH(A) ($v' = 2$), which are predissociated, and even other electronic states, CH(B). The contributions of these states would lower the probability of forming CH(A) in the $v' = 0$ and $v' = 1$ levels, which are the only ones reported here for the $C_2H + O(^3P)$ reaction. Also, it is unlikely that the excess energy of C_2H* would selectively result in vibrational excitation of the CH(A) but not rotational excitation. If one assumes a 1×10^{-10} cm^3 $molecule^{-1}$ s^{-1} hard sphere collision rate for relaxation and takes into consideration that the total pressure is about 100 mTorr (13 Pa), then the average time between collisions is approximately 3 μs. The emission lifetime of the CH(A) state (537 ns) is much shorter than the hard sphere collision time, therefore >99% of the emission from CH(A) can be considered nascent. There is a simple analogy between time-resolved photodissociation experiments and the present experiment with regard to determining nascent product distributions. In a typical photodissociation experiment, the emission of the product is time gated after the laser pulse to eliminate the part of the product emission that originates from molecules that collide later. In the present experiments, collisions are essential to observe the chemiluminescence from reaction products. Instead of gating the emission to the laser, the lifetime of the CH(A) acts as an internal gate for the detection of the CH(A) reaction product. The ratio of the emission lifetime of the CH(A) product and the average time between collisions (pressure) determines how close the observed CH(A) emission states are to nascent.

The CH(A) spectrum consists of three main branches (P, Q, and R), which are split by spin−orbit splitting and Λ doubling.[19] The experimental spectrum in Figure 3 only shows the Q and R branches. In this experiment, an interference filter is used, which does not transmit the entire CH(A) spectrum at frequencies corresponding to the P branch. The separation due to Λ doubling is approximately 0.1 cm^{-1}, which could not be resolved in this experiment. Each line in the R branch is split due to the spin−orbit splitting mentioned before. The spin−orbit splitting is easily observed in the R branch under higher resolution (Figure 4). The rotational populations are not affected by predissociation if the rotational quantum number N' is less than 23 for $v' = 0$ and less than 22 for $v' = 1$.[20]

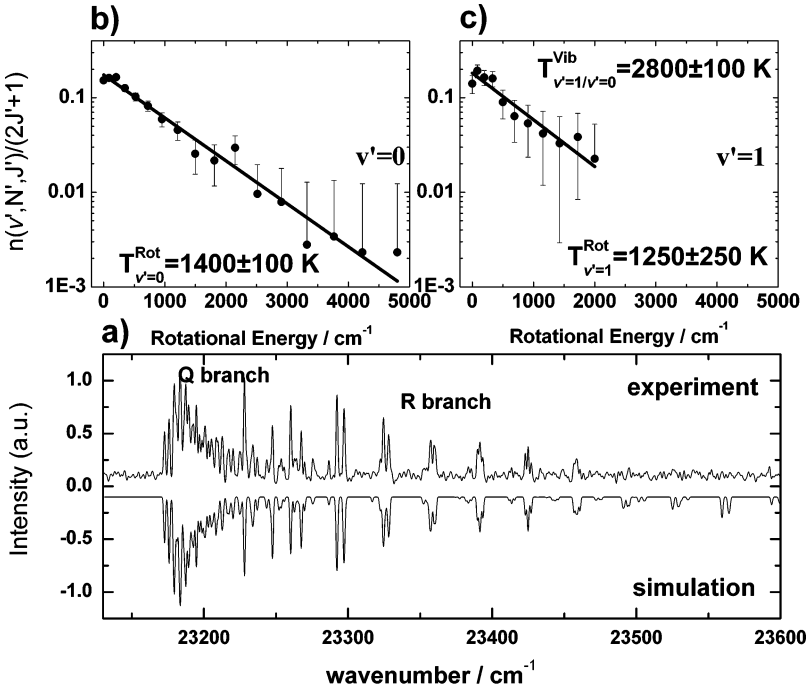

Figure 4. (a) Experimental and simulated spectrum of the CH(A) from $C_2H + O(^3P)$ using the effusive reactor in Figure 1b and the time-resolved apparatus. The data are taken with the high-sensitivity photomultiplier tube at 0.8 cm^{-1} spectral resolution and 2 μs time delay after the laser pulse. The total pressure is 100 mTorr (13 Pa) with the balance due to Ar in the detection volume of the instrument. The laser fluence is 60 mJ cm^{-2} pulse^{-1}. The simulated spectrum is inverted for better visibility. The experimentally determined nascent rotational distribution (solid circles) of CH(A) from $C_2H + O(^3P)$ is shown for $v' = 0$ (b) and $v' = 1$ (c). The solid line indicates the fitting of the experimental nascent distribution with a Boltzmann distribution. The rotational temperatures are found to be 1400 ± 100 K and 1250 ± 250 K. The vibrational temperature is 2800 ± 100 K.

The rotational and vibrational populations are derived by minimizing the error function (F_{error}) between a fitting function (f) and the entire experimental spectrum (F_{data}) in Figure 4.

$$F_{error} = [F_{data} - \int_{-\infty}^{\infty} f(p_i,\tau)g(t-\tau)e^{i\omega\tau}\,d\tau]^2 \qquad (1)$$

The fitting function is generated from known molecular constants,[19] calculated Hönl−London factors,[21] and Franck−Condon factors[22] of the A−X transition of the CH radical indicated by p_i in the equation. The fitting function is convolved with the instrument response function (g). Input parameters of the fitting function (p_i) are the vibrational populations of the CH(A) and the individual rotational populations of each vibrational level. The details of constructing the fitting function have been described previously.[21] The results of the population distributions in Figure 4 are discussed further below.

Microwave Discharge Experiment. It is well-known that in low-pressure C_2H_2/O/H flames there is a significant amount of CH(A) present, which has been attributed to the $C_2H + O(^3P)$ reaction.[6,23] The formation of C_2H in these types of flames can be understood by the following mechanism:[24]

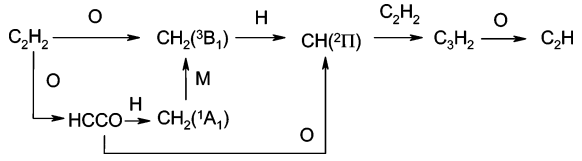

The above mechanism is not chemically balanced; it only indicates the reaction pathways for the formation of C_2H radicals taken directly from the literature.[24] The bottleneck for the formation of C_2H is the formation of the ground-state CH radical. The ground-state CH radical can be formed efficiently via two different pathways as indicated above. Some pathways for the production of C_2H radicals at room temperature also require the presence of H atoms, which are formed through various processes[25] such as

$$C_2H_2 + O \rightarrow HCCO + H \qquad (k = 9.04 \times 10^{-14}\ \text{cm}^3\ \text{molecule}^{-1}\ \text{s}^{-1})$$

$$HCCO + O \rightarrow 2CO + H \qquad (k = 1.03 \times 10^{-10}\ \text{cm}^3\ \text{molecule}^{-1}\ \text{s}^{-1})$$

$$CH_2(^3B_1) + O \rightarrow CO + 2H \qquad (k = 7.08 \times 10^{-11}\ \text{cm}^3\ \text{molecule}^{-1}\ \text{s}^{-1})$$

$$CH_2(^1A_1) + O \rightarrow CO + 2H \qquad (k = 1.3 \times 10^{-10}\ \text{cm}^3\ \text{molecule}^{-1}\ \text{s}^{-1})$$

It has to be pointed out that C_2H radicals can be produced in the absence of H atoms[25] as well, through the following steps

$$HCCO + O \rightarrow CH + CO_2 \qquad (k = 8 \times 10^{-12}\ \text{cm}^3\ \text{molecule}^{-1}\ \text{s}^{-1})$$

$$CH + C_2H_2 \rightarrow C_3H_2 + H \qquad (k = 2 \times 10^{-10}\ \text{cm}^3\ \text{molecule}^{-1}\ \text{s}^{-1})$$

$$C_3H_2 + O \rightarrow C_2H + H + CO \qquad (k = 6.9 \times 10^{-11}\ \text{cm}^3\ \text{molecule}^{-1}\ \text{s}^{-1})$$

The relative importance of the pathways varies with experimental conditions, but previous studies suggest[25] the latter mechanism is important in low-temperature C_2H_2/O/H flames.

In our experiment, O atoms are generated via microwave discharge of oxygen molecules and reacted with C_2H_2 to

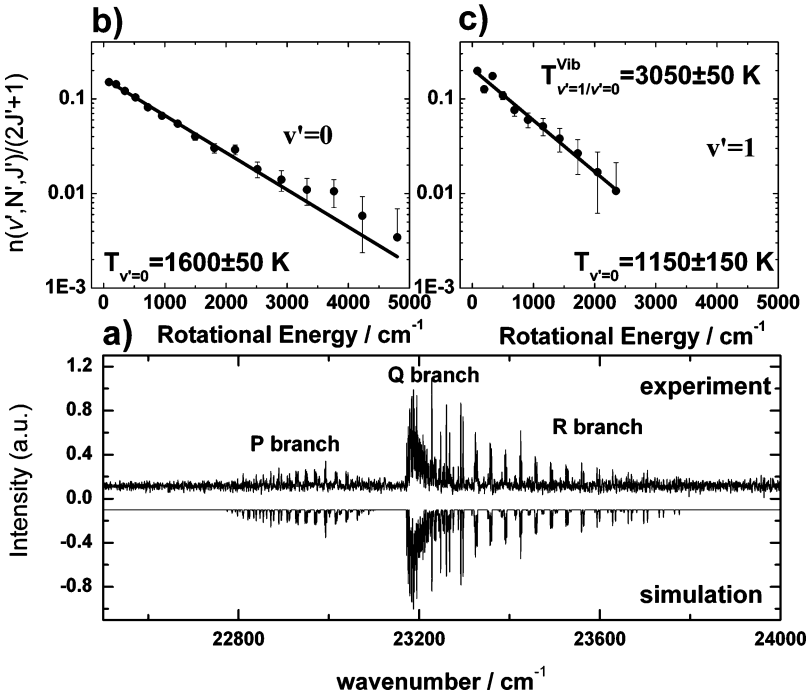

Figure 5. (a) Experimental and simulated spectrum of the CH(A) from $C_2H + O(^3P)$ using the microwave discharge reactor in Figure 1c. The flow rates of O_2, C_2H_2, and Ar are 1000, 100, and 200 sccm, respectively, and p(total) = 150 mTorr (20 Pa). The data are taken with the high-sensitivity photomultiplier tube at 0.8 cm^{-1} spectral resolution. The simulated spectrum is inverted for better visibility. The experimentally determined nascent rotational distribution (solid circles) of CH(A) from $C_2H + O(^3P)$ is shown for $v' = 0$ (b) and $v' = 1$ (c). The solid line indicates the fitting of the experimental nascent distribution with a Boltzmann distribution. The rotational temperatures are found to be 1600 ± 50 K and 1150 ± 150 K. The vibrational temperature is 3050 ± 50 K.

simulate the conditions present in the C_2H_2/O/H flames. Figure 5 shows the observed CH(A) spectrum from the reaction of C_2H_2 with microwave discharge generated O atoms under low-pressure conditions (~150 mTorr, 20 Pa). It is assumed that the C_2H is generated according to the above pathways and it reacts with O atoms resulting in the CH(A) emission. The mechanism has been confirmed at 600 K,[24] but a similar mechanism is expected at room temperature as well.[25] The CH(A) emission is observed only after 1 cm downstream from the initial mixing of C_2H_2 and O atoms, which supports the idea that the C_2H is only formed in a later step such as the mechanisms presented above. The pressure is low enough to obtain the nascent (or close to nascent) rotational and vibrational distributions of the CH(A) product (see argument in previous section). In addition, several low-resolution (4 cm^{-1}) spectra were taken at varying total pressures (150−800 mTorr). The change in the total pressure is achieved by introducing more Ar buffer gas, and this does cause deactivation of the higher rotational states at higher pressures. In the microwave discharge experiment at pressures lower than 150 mTorr total, no significant CH(A) emission is observed.

The analysis of the vibrational and rotational populations of CH(A) from the microwave experiment shows that the rotational temperatures in the $v' = 0$ and $v' = 1$ states are 1600 ± 100 K and 1150 ± 150 K, respectively. The CH(A) from the laser-excited photodissociation experiment has similar values (1400±100 K and 1250 ± 200 K, respectively), although the average fraction of energy channeled into rotation is a little less. The comparison of the vibrational temperatures of these two experiments also shows a similar trend (3050 ± 50 K microwave vs 2800 ± 100 K photodissociation). The results corroborate that the CH(A) emission from the photodissociation experiment and the CH(A) emission from the microwave discharge experiment come from the same process ($C_2H + O(^3P)$). The slight differences can probably be attributed to factors such as the different amount of initial vibrational and electronic excitation of C_2H in the photolysis experiment, slight differences in pressures (different rotational and vibrational deactivation, if any), and the possibility that some portion of the CH(A) may be the result of another reaction, such as $C_2H + O_2$. The $C_2H + O_2$ reaction does occur; however, the room-temperature rate coefficient of this reaction[7] is 500 times less than that of $C_2H + O(^3P)$. The contribution of the $C_2H + O_2$ reaction could be comparable depending on the O atom density.[26] The exothermicity of the $C_2H + O_2$ reaction is, however, about two times greater than $C_2H + O$, which might result in higher rotational and vibrational temperatures. On the other hand, the other product of the $C_2H + O_2$ reaction is CO_2, in contrast to the CO product in the $C_2H + O$ reaction. The CO_2 could lead to a smaller average energy partitioned into the CH(A) product based on simple equipartition considerations (CO_2 has more degrees of freedom than CO). Given these ambiguities, it is unlikely that a more detailed comparison of the photodissociation and microwave experiments is valuable. Therefore, the dynamical results are discussed primarily in the context of the time-resolved photodissociation measurements.

Dynamics of the CH(A) Channel of the $C_2H + O(^3P)$ Reaction. The HCCO (ketenyl) radical has been previously suggested as the most likely reaction intermediate for the $C_2H + O$ reaction.[6,7] To understand better the dynamics of the $C_2H + O$ reaction, several models are considered: first, an impulsive model[27] where the energy is released between the CC bond and is deposited into translation, vibrations, and rotations determined by the geometry of the intermediate and reduced masses of the fragments and second, a simple statistical model, in which all the energetically allowed states are equally probable. Deviation from a statistical distribution can be attributed directly to dynamical effects of the reaction. These two models represent the two ends of the spectrum between the complete randomization of available energy between dif-

ferent degrees of freedom vs the localization of available energy into a particular degree of freedom. The results below show that neither of these models sufficiently describe the dynamics of the $C_2H + O$ reaction, and a third model is considered, in which the bond length changes in the intermediate vs the final products could also affect the observed product distributions.

For the impulsive model, an HCCO intermediate is assumed. The linear momentum of the dissociating CC bond is released into translation, vibration, and rotation of the fragments without reaching equilibrium in their internal degrees of freedom. The departing C atoms undergo inelastic collisions with the rest of the molecule, which result in energy transfer. The model uses simple classical mechanics based on torques and forces to estimate the relative distribution of energy among the different internal degrees of freedom. The translational energy released (E_{Trans}) into the fragments from the total available energy ($E_{Avl} = 5100$ cm^{-1} if the CH(A) state is formed) is the ratio of the reduced masses of C and C (μ_a) and the reduced mass of the fragments CH and CO (μ_f) given by

$$E_{Trans} = \frac{\mu_a}{\mu_f} E_{Avl} \tag{2}$$

The rest of the energy is distributed into the internal degrees of freedom. The ratio of the rotational (E_{Rot}) vs vibrational (E_{Vib}) energy release is a function of the angle (χ) between the CC bond and CH bond.

$$E_{Vib} = \left(1 - \frac{\mu_a}{\mu_f}\right) E_{Avl} \cos^2 \chi \tag{3}$$

$$E_{Rot} = \left(1 - \frac{\mu_a}{\mu_f}\right) E_{Avl} \sin^2 \chi \tag{4}$$

Similar equations will apply to the CO fragments as well. A more rigorous explanation of the model can be found in Trentelman et al.[27]

The statistical model is based on the equipartition theorem. The translational degrees of freedom carry $^3/_2kT$, and the vibrational and rotational degrees of freedom carry kT in the case of a diatomic. The total energy is equal to

$$E_{Total} = E_{Trans} + E_{Rot} + E_{Vib} = \frac{3}{2}kT + kT + kT \tag{5}$$

The classical equipartition theorem assumes that the energy level spacing is much smaller than the available energy, which is not correct in this experiment. The total available energy is 5100 cm^{-1}, which is comparable to the vibrational spacing of CH (2930 cm^{-1}) and CO (2169 cm^{-1}). Results that are more accurate can be obtained by direct counting of the available states.[28] The prior probability distribution ($P^0(E_i;E)$) of a particular internal degree of freedom for a general case can be described by the following equation

$$P^0(E_i;E) = \frac{g_i[E - E_i]^{1/2}}{\sum_i g_i[E - E_i]^{1/2}} \tag{6}$$

where E is the total available energy, E_i is the energy of the vibration or rotation of the fragments, and g_i is the degeneracy factor. Taking the average of the individual values of $P^0(E_i; E)$ would result in the average fraction of energy ($\langle E_i \rangle$) disposed into a particular degree of freedom

$$\langle E_i \rangle = \sum_i E_i P^0(E_i;E) \tag{7}$$

TABLE 1: Results of Experiments and Models for the Partitioning of Energy for the $C_2H + O$ Reaction

	impulsive model (cm^{-1})				
	$\chi = 180°$, $\chi' = 180°$	$\chi = 90°$, $\chi' = 90°$	statistical (cm^{-1})	direct count (cm^{-1})	experiment (cm^{-1})
$\langle E_{Trans}(CH) \rangle$	2353	2353	1092	1335	
$\langle E_{Vib}(CH) \rangle$	196	0	728	242	540 ± 20
$\langle E_{Rot}(CH) \rangle$	0	196	728	890	900 ± 50
$\langle E_{Trans}(CO) \rangle$	1092	1092	1092	1335	
$\langle E_{Vib}(CO) \rangle$	1457	0	728	405	(1300)[10]
$\langle E_{Rot}(CO) \rangle$	0	1457	728	890	

In these calculations, a rigid rotor, harmonic oscillator approximation is used. This approximation is considered good in this particular case, since only a few v' values can be populated and at these lower vibrational levels the contribution of anharmonicity is negligible. The results from both statistical models and the impulsive model for two different HCCO geometries, along with the experimentally determined values, are summarized in Table 1.

The experimental average energy for CH vibration is obtained by multiplying the vibrational population in $v' = 1$ by 2930 cm^{-1}, which would result in 540 cm^{-1} since only two vibrational levels are accessible. Notice that the experimental vibrational temperature is 2800 K, but this does not result in a value of 1940 cm^{-1} because of the limited set of levels. This simple calculation demonstrates that the direct count does not achieve the same energy predicted by the equipartition theorem. The other experimental values are calculated in a similar way.

The experimentally determined rotational population of CH shows remarkably good agreement with the statistical prediction (900 cm^{-1} vs 890 cm^{-1}), which strongly suggests that the HCCO complex exists long enough that the vibrational modes of HCCO and the resulting rotational energy in the fragments may be completely randomized. The vibrational populations show a strong deviation from the statistical based on direct count (540 cm^{-1} vs 242 cm^{-1}), which could indicate a dynamical aspect of the $C_2H + O(^3P)$ reaction. Comparison of the vibrational and rotational energy disposal from the impulsive model at several different angles suggests that this model cannot account for the relatively large energy content of the vibrational or rotational degrees of freedom of the CH fragment. This comparison is independent of the geometry of the HCCO fragment. The explanation for this is simply that the CH has a small reduced mass, therefore, the efficiency of energy transfer from the bond dissociation into the internal degrees of the CH is negligible. This is also seen in the table, which indicates the small internal energy (196 cm^{-1}) channeled into the CH if the impulsive model is used. A similar argument can be made for the CO fragment, however, the reduced mass of the CO is much larger and the impulsive energy release, in principle, could account for the large vibrational energy release. The vibrational energy release of the CO for the $C_2H + O(^3P)$ reaction[10] was determined from the nascent IR emission spectrum of CO. It has to be pointed out that the determination of the average energy disposal into CO in that experiment may contain a large error, because the ground-state population of the CO is not known, but it is extrapolated from the higher vibrational levels. The poor fit of the results of the models for CH(A) may suggest that the relatively high vibrational energy content of the CH

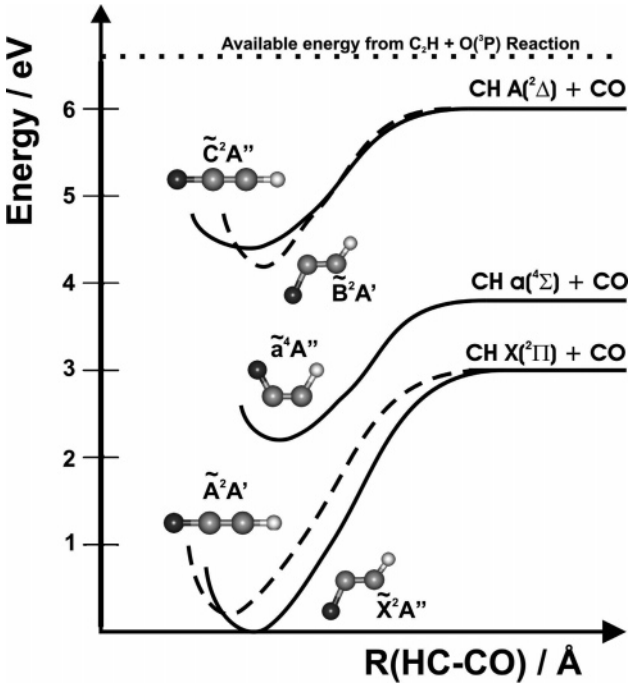

Figure 6. Simple scheme of the adiabatic potential energy surfaces of HCCO along the CH−CO reaction coordinate indicating the possible exit channels. The figure is based on Mordaunt et al.[32]

fragment may be the result of other factors such as the geometry changes in the transition state to the final products.

Theoretical calculations of the ketenyl radicals show that the CH bond distance in the different electronic states ranges between (1.06−1.08 Å).[29−31] Compared to the CH radical (1.10 Å), the bond distances definitely change, which could account for the preferential energy release into vibrations. If the barrier or transition state is close to the exit channel, then the separation along the CC bond could effectively dispose of internal energy into the CH vibrations, leading to the high vibrational excitation of the CH product. A similar argument applies to the CO fragment. The bond distances of CO in the fragment (1.13 Å) and the HCCO (1.16−1.18 Å) show changes that are even more significant. These calculations also indicate that the bond distance in the CH fragment is expanding compared to the values in the different electronic states of the HCCO, while the bond distance in the CO fragment is contracting.

The potential energy curves of the HCCO intermediate along the CC bond dissociation coordinate[32] are shown in Figure 6. Devriendt et al.[6,7] suggested that the relatively high yield of CH(A) can be explained by a path through the ground electronic state of the HCCO radical. They suggested that the rotational motion of the high-energy content bent intermediate would couple to the nuclear angular momentum, which would result in the electronic A state of CH (higher electronic angular momentum). However, the available energy of the reaction (6.4 eV relative to the ground-state HCCO) also makes the formation of electronically excited HCCO radicals probable. The two electronically excited HCCO intermediates are the bent HCCO ($\tilde{B}$) and the linear HCCO ($\tilde{C}$). The recently observed branching ratio[10] for the CH(X) + CO and CH(A) + CO branches from C_2H + $O(^3P)$ shows that a relatively large portion of the branching favors the CH(A) + CO channel, which could further support the possible role of excited electronic states of the HCCO intermediate. On the basis of the data available, no definite assignment can be made here whether the linear or the bent excited electronic state of the HCCO would result in the observed state distributions. The approximate Boltzmann rotational distribution of CH(A) observed here suggests that there is still a bound intermediate involved, which would make the linear $\tilde{C}$ state or bent $\tilde{B}$ state of the HCCO the most likely electronically excited states for the production of CH(A) from the C_2H + $O(^3P)$ reaction.

The photodissociation of HCCO at 266 nm[33] reveals that the resulting CH(X) is rotationally highly excited. In that experiment, the excitation takes place in the $\tilde{B}$ state of the HCCO but with insufficient energy to result in electronically excited CH(A). In addition, the absorption spectrum of the $\tilde{B}$ state of HCCO shows broadening at energies higher than 4.3 eV due to the predissociation of the HCCO.[34] This suggests that the bound $\tilde{B}$ state (bent $\tilde{B}^2A'$) of the HCCO can couple mainly to the CH(X) + CO exit channel in agreement with the observation of the rotationally hot CH(X) product.[33] Finally, there is the spin-forbidden CH(a) + CO channel,[32,35] but the significance of this channel is less at high energies in these experiments.

This study shows that the CH(A) fluorescence is a suitable probe to obtain detailed information about the state-resolved dynamics of the C_2H + $O(^3P)$ reaction using FTVIS spectroscopy. Comparison between experiment and theory suggests that the lifetime of the $HCCO^{\ddagger}$ reaction intermediate may be sufficiently long to allow the randomization of available energy, however, the preferential vibrational energy disposal of the C_2H + $O(^3P)$ reaction into the CH(A) vibrations may be due to bond length changes in the transition state. To clarify the mechanism of the C_2H + $O(^3P)$ reaction further and to resolve the possible discrepancies, studies of the photodissociation of the HCCO radical at higher excitation energies will be valuable.

Acknowledgment. This work has been supported by the U.S. Department of Energy under the Contract #DE-AC02-05CH11231.

References and Notes

(1) Bass, A. M.; Broida, H. P. *NBS Monogr.* **1961**, *24*.
(2) Gaydon, A. G. *The Spectroscopy of Flames*, 2nd ed.; Chapman and Hall: London, 1974.
(3) Gaydon, A. G.; Wolfhard, H. G. *Flames*; Chapman and Hall: London, 1960.
(4) Brenig, H. H. Ph.D. Thesis, Wuppertal, Germany, 1981.
(5) Brennen, W.; Carringt. T. *J. Chem. Phys.* **1967**, *46*, 7.
(6) Devriendt, K.; Peeters, J. *J. Phys. Chem. A* **1997**, *101*, 2546.
(7) Devriendt, K.; Van Look, H.; Ceursters, B.; Peeters, J. *Chem. Phys. Lett.* **1996**, *261*, 450.
(8) Renlund, A. M.; Shokoohi, F.; Reisler, H.; Wittig, C. *J. Phys. Chem.* **1982**, *86*, 4165.
(9) Renlund, A. M.; Shokoohi, F.; Reisler, H.; Wittig, C. *Chem. Phys. Lett.* **1981**, *84*, 293.
(10) Chikan, V.; Nizamov, B.; Leone, S. R. *J. Phys. Chem. A* **2004**, *108*, 10770.
(11) Carl, S. A.; Nguyen, H. M. T.; Nguyen, M. T.; Peeters, J. *J. Chem. Phys.* **2003**, *118*, 10996.
(12) Chikan, V.; Leone, S. R. *J. Phys. Chem. A* **2004**, *109*, 2525.
(13) Sorkhabi, O.; Blunt, V. M.; Lin, H.; Xu, D. D.; Wrobel, J.; Price, R.; Jackson, W. M. *J. Chem. Phys.* **1997**, *107*, 9842.
(14) Griffiths, P. R. *Fourier transform infrared spectrometry*; Wiley: New York, 1986.
(15) Blitz, M. A.; Heard, D. E.; Pilling, M. J.; Arnold, S. R.; Chipperfield, M. P. *Geophys. Res. Lett.* **2004**, *31*.
(16) Yamanouchi, K.; Takeuchi, S.; Tsuchiya, S. *J. Chem. Phys.* **1990**, *92*, 4044.
(17) Fletcher, T. R.; Leone, S. R. *J. Chem. Phys.* **1989**, *90*, 871.
(18) Hsu, Y. C.; Chen, F. T.; Chou, L. C.; Shiu, Y. J. *J. Chem. Phys.* **1996**, *105*, 9153.
(19) Zachwieja, M. *J. Mol. Spectrosc.* **1995**, *170*, 285.
(20) Lindner, J.; Ermisch, K.; Wilhelm, R. *Chem. Phys.* **1998**, *238*, 329.
(21) Baas, R. C.; Beenakker, C. I. M. *Comput. Phys. Commun.* **1974**, *8*, 236.
(22) Garland, N. L.; Crosley, D. R. *JQSRT* **1985**, *33*, 591.
(23) Sheaffer, P. M.; Zittel, P. F. *J. Phys. Chem. A* **2000**, *104*, 10194.
(24) Boullart, W.; Devriendt, K.; Borms, R.; Peeters, J. *J. Phys. Chem.* **1996**, *100*, 998.

(25) Peeters, J.; Langhans, I.; Boullart, W.; Nguyen, M. T.; Devriendt, K. *J. Phys. Chem.* **1994**, *98*, 11988.

(26) Granier, A.; Pasquiers, S.; Boisselaporte, C.; Darchicourt, R.; Leprince, P.; Marec, J. *J. Phys. D: Appl. Phys*. **1989**, *22*, 1487.

(27) Trentelman, K. A.; Kable, S. H.; Moss, D. B.; Houston, P. L. *J. Chem. Phys.* **1989**, *91*, 7498.

(28) Muckerman, J. T. *J. Phys. Chem.* **1989**, *93*, 179.

(29) Sattelmeyer, K. W.; Yamaguchi, Y.; Schaefer, H. F. *Chem. Phys. Lett.* **2004**, *383*, 266.

(30) Szalay, P. G.; Fogarasi, G.; Nemes, L. *Chem. Phys. Lett.* **1996**, *263*, 91.

(31) Szalay, P. G.; Stanton, J. F.; Bartlett, R. J. *Chem. Phys. Lett.* **1992**, *193*, 573.

(32) Mordaunt, D. H.; Osborn, D. L.; Choi, H.; Bise, R. T.; Neumark, D. M. *J. Chem. Phys.* **1996**, *105*, 6078.

(33) Carl, S. A.; Sun, Q.; Peeters, J. *J. Chem. Phys.* **2001**, *114*, 10332.

(34) Brock, L. R.; Mischler, B.; Rohlfing, E. A. *J. Chem. Phys.* **1999**, *110*, 6773.

(35) Osborn, D. L.; Mordaunt, D. H.; Choi, H.; Bise, R. T.; Neumark, D. M.; Rohlfing, C. M. *J. Chem. Phys*. **1997**, *106*, 10087.